Fibroblast Activation Protein–Targeted Radioligand Therapy for Treatment of Solid Tumors

Spencer D. Lindeman[1], Ramesh Mukkamala[1], Autumn Horner[1], Pooja Tudi[1], Owen C. Booth[1], Roxanne Huff[1], Joshua Hinsey[1], Anders Hovstadius[1], Peter Martone[1], Fenghua Zhang[1], Madduri Srinivasarao[1], Abigail Cox[2], and Philip S. Low[1]

[1]Department of Chemistry and Institute for Drug Discovery, Purdue University, West Lafayette, Indiana; and [2]Department of Comparative Pathobiology, Purdue College of Veterinary Medicine, West Lafayette, Indiana

Fibroblast activation protein (FAP) has received increasing attention as an oncologic target because of its prominent expression in solid tumors but virtual absence from healthy tissues. Most radioligand therapies (RLTs) targeting FAP, however, suffer from inadequate tumor retention or clearance from healthy tissues. Herein we report a FAP-targeted RLT comprising an FAP6 ligand conjugated to DOTA and an albumin binder (4-p-iodophenylbutyric acid, or IP) for enhanced pharmacokinetics. We evaluated the performance of the resulting FAP6-IP-DOTA conjugate in 4 tumor models, 3 of which express FAP only on cancer-associated fibroblasts, that is, analogously to human tumors. **Methods:** Single-cell RNA-sequencing data were analyzed from 34 human breast, ovarian, colorectal, and lung cancers to quantify FAP-overexpressing cells. FAP6-DOTA conjugates were synthesized with or without an albumin binder (IP) and investigated for binding to human FAP-expressing cells. Accumulation of ^{111}In- or ^{177}Lu-labeled conjugates in KB, HT29, U87MG, and 4T1 murine tumors was also assessed by radioimaging or biodistribution analyses. Radiotherapeutic potency was quantitated by measuring tumor volumes versus time. **Results:** Approximately 5% of all cells in human tumors overexpressed FAP (cancer-associated fibroblasts comprised ~77% of this FAP-positive subpopulation, whereas ~2% were cancer cells). FAP6 conjugates bound to FAP-expressing cells with high affinity (dissociation constant, ~1 nM). ^{177}Lu-FAP6-IP-DOTA achieved an 88-fold higher tumor dose than ^{177}Lu-FAP6-DOTA and improved all tumor–to–healthy-organ ratios. Single doses of ^{177}Lu-FAP6-IP-DOTA suppressed tumor growth by about 45% in all tested tumor models without causing reproducible toxicities. **Conclusion:** We conclude that ^{177}Lu-FAP6-IP-DOTA constitutes a promising candidate for FAP-targeted RLT of solid tumors.

Key Words: radioligand therapy; FAP; albumin binder; scRNA-seq; cancer-associated fibroblasts

A subset of cancer-associated fibroblasts (CAFs) is characterized by expression of a cell-surface serine protease termed fibroblast activation protein (FAP) that participates in remodeling of the extracellular matrix during tumor growth and metastasis (1). Approximately 90% of epithelial cancers upregulate FAP (2), and FAP-targeted PET tracers have been shown to image at least 28 different cancer types in humans (3). Because of FAP's broad expression on CAFs and its nearly complete absence from healthy tissues, FAP has recently been explored as a receptor for targeted radioligand therapy (RLT) in a diversity of solid tumors (4,5).

Optimal FAP-targeted radiotherapy might be expected to satisfy several criteria. First, it will contain a therapeutic radionuclide that effectively irradiates multiple cancer cells near each CAF. Second, the targeting ligand will possess high affinity and specificity for FAP to minimize uptake by its homologs in healthy organs. Third, the pharmacokinetic properties of the resulting conjugate will be optimized to ensure prolonged tumor accumulation and rapid clearance from normal tissues.

To achieve these objectives, we first derivatized a new FAP-targeting ligand (FAP6) with DOTA via a polyethylene glycol spacer. We then incorporated the established albumin binder 4-p-iodophenylbutyric acid (IP) (6) into our FAP-targeting radioligand (Fig. 1), since such appendages have been observed to prolong the pharmacokinetics and improve tumor uptake of RLTs (7–10). We demonstrate here that the resulting conjugate, FAP6-IP-DOTA, exhibits high FAP affinity, prolonged circulation, increased tumor uptake, and minimal retention in healthy tissues. Moreover, the final ^{177}Lu-labeled RLT causes no obvious toxicity to healthy tissues while achieving significant anticancer efficacy in 4 different murine tumor models.

MATERIALS AND METHODS

Reagents, vendors, syntheses, and full experimental procedures are detailed in the supplemental materials (available at http://jnm.snmjournals.org).

Single-Cell RNA-Sequencing (scRNA-Seq) Analysis

We analyzed scRNA-seq data collected on fresh human tumor samples; the results of this analysis were reported elsewhere previously (11). FAP gene expression was extracted, quantitated, and plotted on a log(2) scale for comparison among different cell types in each cancer tissue, according to online tutorials (12).

Cell Culture and Transduction

4T1, KB, HT29, and U87MG cells were purchased from American Type Culture Collection and cultured as reported previously (13,14). HEK-293T cells with high levels of FAP expression (HEK-hFAP) were generated as formerly described (13).
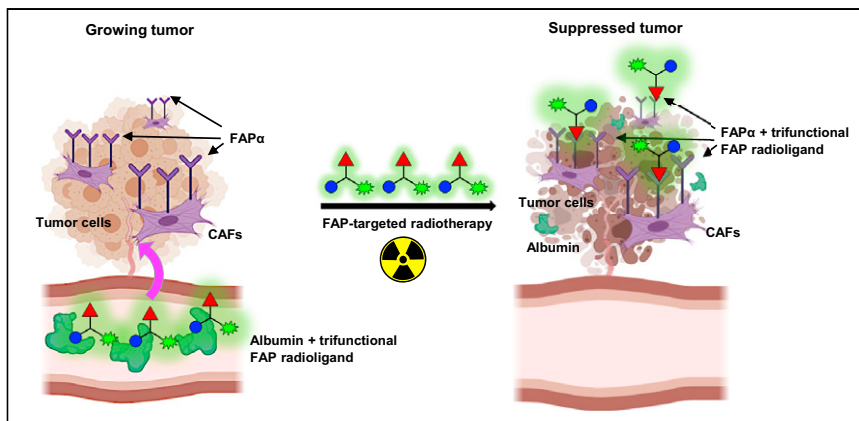
Radiolabeling

FAP6 conjugates were diluted in ammonium acetate (0.5 M, pH 8.0). ^{111}In[InCl$_3$] (Cardinal Health) was added to obtain a specific activity of

FIGURE 1. Circulation of radiolabeled FAP6-IP-DOTA is prolonged because of affinity of iodophenyl-butyric acid (blue circles) for serum albumin. This enables conjugate to perfuse poorly vascularized solid tumors so that ligand (red triangles) may bind to FAP receptors on CAFs. Chelated radionuclide (green symbols) emits radiation that induces DNA-strand breaks inside tumor cells, thereby suppressing tumor growth.

no more than 4.0 MBq/nmol, or ^{177}Lu[LuCl$_3$] (RadioMedix) was added to obtain a specific activity of no more than 11.0 MBq/nmol. The resulting solutions were heated to 90°C for 10–20 min, and the radiopurities of the products were analyzed by radio–high-performance liquid chromatography. Radiopurity exceeded 95% in all studies.

Cell Binding Studies

Flow Cytometry. Antihuman FAP antibody conjugated to allophycocyanin dye was used for staining all cell lines except 4T1 cells, which were stained with antimouse FAP antibody and then a secondary allophycocyanin-conjugated antibody.

Displacement Assay. HEK-hFAP cells grown to confluency in 24-well plates were coincubated with FAP6-rhodamine and increasing concentrations of FAP6-DOTA or FAP6-IP-DOTA. The cells were then washed, dissolved, and analyzed by a fluorescent plate reader.

Binding Assay. Hs894 CAFs grown to confluency in 24-well plates were incubated with increasing concentrations of ^{111}In-FAP6-DOTA or ^{111}In-FAP6-IP-DOTA in the absence or presence of an excess of FAP6 ligand. The cells were then washed, dissolved, and analyzed by a γ-counter.

Animal Husbandry

The mice were provided normal rodent chow and water ad libitum and maintained on a standard 12-h light–dark cycle. All animal procedures were approved by the Purdue Animal Care and Use Committee.

Tumor Models

BALB/c mice were inoculated on their shoulder with 1×10^5 4T1 cells. Nu/nu mice were inoculated on their shoulder with 5×10^6 HT29, KB, or U87MG cells.

SPECT/CT Scans

Tumor-bearing mice were intravenously injected with FAP6 conjugate radiolabeled with about 13 MBq of ^{111}In. At indicated times, the mice were anesthetized and then scanned using an MILabs VECTor/CT instrument. CT scans were reconstructed using NRecon software (Micro Photonics Inc.). The datasets were fused, filtered, and processed using PMOD software (version 3.2).

Radioactive Biodistribution

Tumor-bearing mice ($n = 3$–5) were intravenously injected with ^{177}Lu-FAP6-DOTA or ^{177}Lu-FAP6-IP-DOTA. At indicated times, the

mice were euthanized, and organs of interest were harvested, weighed, and analyzed by a γ-counter.

Radiotherapy

Mice bearing 4T1, HT29, KB, or U87MG tumors were randomly divided into control and treatment groups to ensure equal starting tumor volumes. Each cohort received a single intravenous injection of either vehicle alone or vehicle with ^{177}Lu-radiolabeled FAP6 conjugate on day 0. Tumors were measured with a caliper in 2 perpendicular directions every other day. The mice were euthanized on reaching one of the predefined endpoint criteria according to the regulations of the Institutional Animal Care and Use Committee.

Toxicology

The mice were weighed every other day during radiotherapy as a gross evaluation of health. Tissue sections from organs of interest ($n = 1$–8 per organ per mouse) were preserved and examined for lesions in a masked manner by a board-certified veterinary pathologist.

Statistical Analysis

Data were analyzed using GraphPad Prism, version 8, unless otherwise stated. All results are presented as mean $\pm$ SE.

RESULTS

scRNA-Seq Analysis of FAP Gene Expression in Multiple Human Tumor Types

To better understand how FAP might serve as a target for RLT, we first sought to quantify cells in human tumors that upregulate FAP expression. For this purpose, FAP gene expression data (Fig. 2) were extracted from a curated database containing scRNA-seq analyses of tumors from 14 breast, 5 ovarian, 7 colorectal, and 8 lung cancer patients (*11*). Quantification of the scRNA-seq data (Supplemental Fig. 1) revealed that about 30% of all CAFs overexpress FAP RNA. Although about 10% of endothelial cells also overexpressed FAP RNA, only about 2% of cancer cells and less than 1% of all other cell types upregulated FAP gene expression. Moreover, about 77% of all FAP-overexpressing cells in the average tumor were fibroblasts, suggesting that animal models used for evaluation of FAP-targeted RLTs should derive their FAP-positive cell population primarily from CAFs. And because FAP-overexpressing cells constituted no more than 10% of all cells in the average cancer mass (mean, 5%), a radionuclide with a large killing radius (e.g., ^{177}Lu) was deemed prudent for effective FAP-targeted radiotherapy. The variability of FAP expression among different human tumor types further suggested that adjusted doses of radioactivity might be necessary to achieve effective therapeutic responses in different patients.

Binding of FAP6 Conjugates to Different Cell Lines

Because FAP was not overexpressed on most human cancer cells, we mimicked FAP expression in human tumors more accurately by selecting cancer cell lines that did not directly express FAP. As documented in Figure 3A, flow cytometry analyses of 4T1, KB, and HT29 cells using species-specific anti-FAP antibodies demonstrated no FAP expression, even though the same cancers are shown to be FAP-positive in murine tumor models
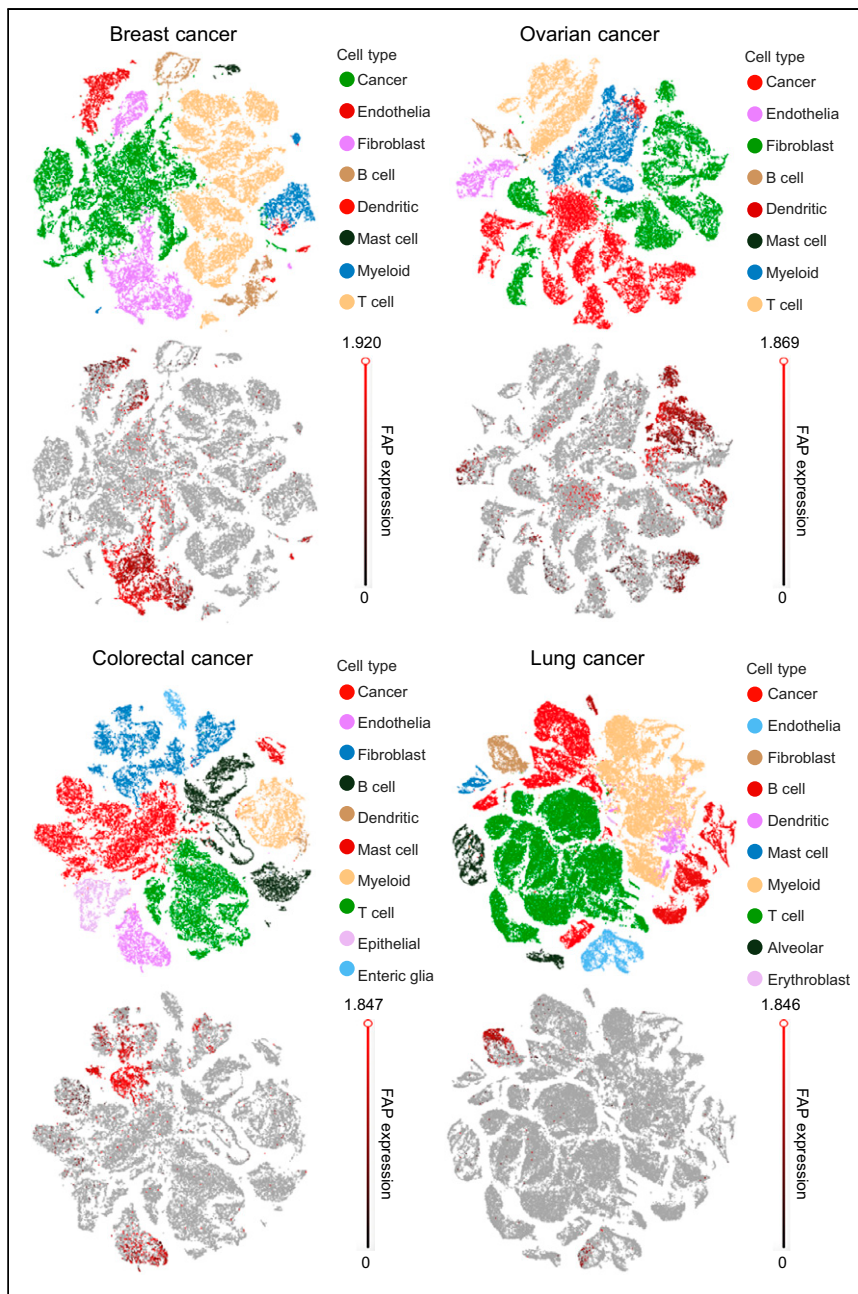
FIGURE 2. t-distributed stochastic-neighbor-embedding plots of scRNA-seq data from human breast, ovarian, colorectal, and lung cancers.

(Supplemental Fig. 2) because of infiltration of CAFs (*13–17*). In contrast, fibroblast cell lines Hs894 and WI38, as well as the glioblastoma cell line U87MG, displayed similarly low levels of endogenous FAP expression. HEK293 cells that do not naturally express FAP were transduced to express artificially high levels of human FAP for use as a positive control.
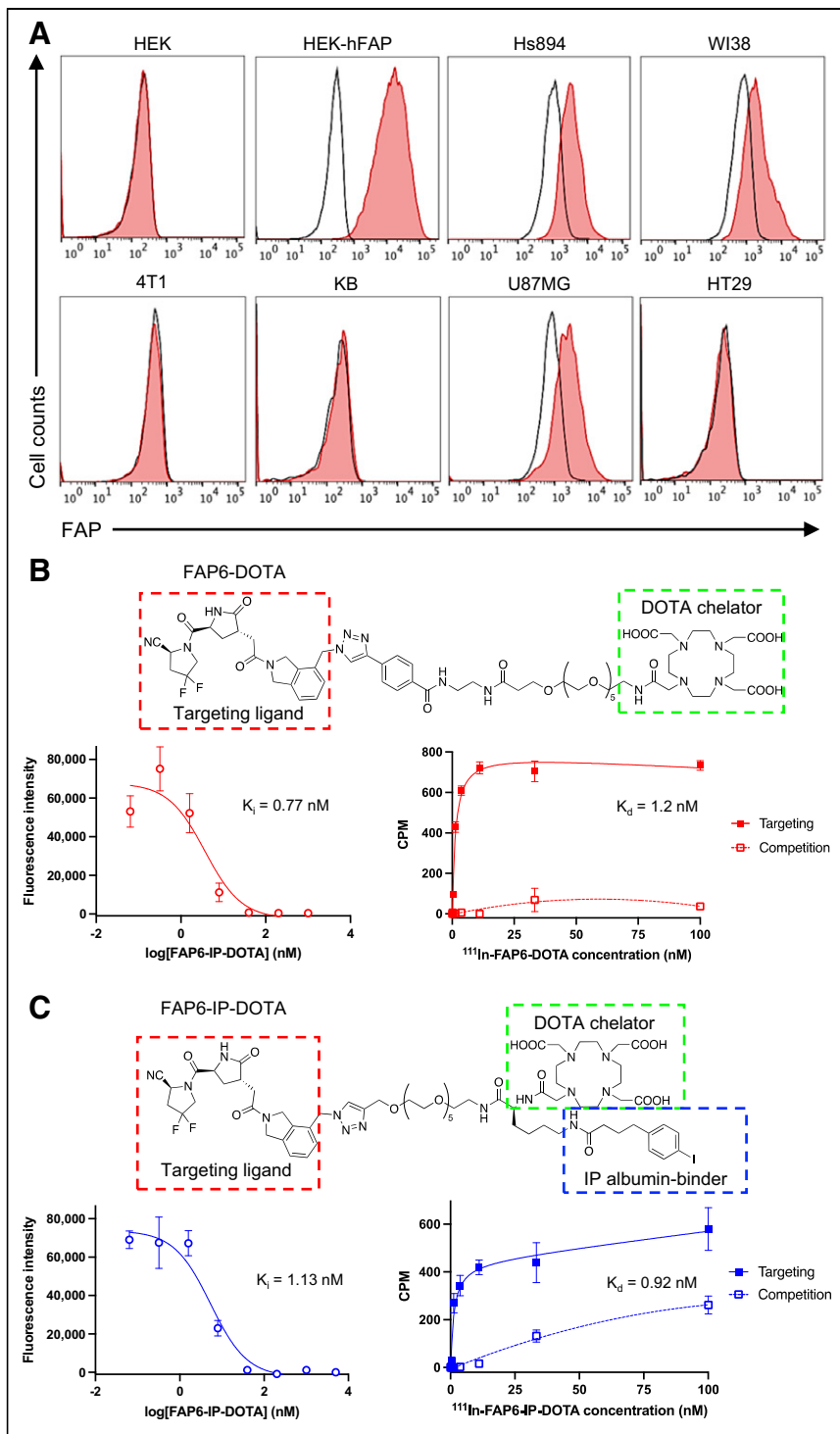
To develop a FAP ligand that can mediate protracted retention of FAP-targeted RLTs in solid tumors, we identified a FAP inhibitor comprising a scaffold different from that of the quinoline-based ligands most used to date (*17–23*). The FAP6 ligand contains a pyroglutamic-isoindoline–based moiety (*13,24*), which is reported to possess higher selectivity for FAP than PREP (a ubiquitously

expressed homolog) (*24*) and longer retention in tumors when conjugated to a near-infrared dye (*13,25*). We then linked FAP6 with DOTA via a polyethylene glycol spacer to yield the FAP6-DOTA conjugate (Supplemental Scheme 1). To evaluate the merit of attaching an albumin binder to FAP6-DOTA, an iodophenyl butyric acid (IP) moiety was inserted to generate FAP6-IP-DOTA (Supplemental Scheme 2). The final structures of FAP6-DOTA (Fig. 3B) and FAP6-IP-DOTA (Fig. 3C) were characterized by liquid chromatography–mass spectrometry (Supplemental Fig. 3). Radiolabeling with ^{111}In and ^{177}Lu was evaluated by radio–high-performance liquid chromatography (Supplemental Fig. 4).

To obtain an initial estimate of the affinity of the FAP6 ligand for FAP, competitive displacement and direct binding curves were generated with both conjugates (Figs. 3B and 3C) in HEK-hFAP and Hs894 CAFs, respectively. FAP6-DOTA and FAP6-IP-DOTA exhibited affinities of about 1 nM for FAP in both cell lines, suggesting that appending the albumin binder did not significantly affect conjugate affinity. Binding was competitively suppressed by coincubation with a 100-times excess of FAP6 ligand, confirming that targeting of FAP6 conjugates to FAP-positive cells was receptor-mediated. Both FAP6 conjugates were also found to internalize into FAP-positive cells (Supplemental Fig. 5), mirroring FAP6-dye conjugates (*13*).

Tumor Accumulation and Biodistribution of FAP6 Radioligands

To determine whether insertion of the albumin binder improves accumulation of FAP6 conjugates in solid tumors, we next compared the biodistributions of both radioligands in tumor-bearing mice wherein the primary FAP-positive cells were CAFs. BALB/c mice inoculated with FAP-negative 4T1 cancer cells were intravenously injected with either ^{111}In-FAP6-DOTA or ^{111}In-FAP6-IP-DOTA for radioimaging (Supplemental Figs. 6–7 show studies to optimize mass doses). The SPECT/CT scans demonstrated high uptake of ^{111}In-FAP6-DOTA in the liver but negligible accumulation in the tumors at 2 and 4 h after injection (Fig. 4A), presumably because of rapid excretion of ^{111}In-FAP6-DOTA before its perfusion into poorly vascularized 4T1 tumors. In contrast, radioimages of mice injected with the same dose of ^{111}In-FAP6-IP-DOTA showed prominent tumor uptake that persisted for at least 120 h after injection (Fig. 4B). Additional SPECT/CT scans of HT29, KB, and U87MG tumors demonstrated the versatility of ^{111}In-FAP6-IP-DOTA tumor targeting and retention (Supplemental Figs. 7 and 8). Competition and untargeted radioimages confirmed that in vivo tumor uptake was FAP-mediated (Supplemental Fig. 9). Although

FIGURE 3. (A) Histograms of FAP expression by indicated cell lines (unstained controls = black; anti-FAP stained cells = red). (B and C) Structures, HEK-hFAP competition assays, and Hs894 CAF binding assays of FAP6-DOTA (B) and FAP6-IP-DOTA (C). K_i = inhibition constant; K_d = dissociation constant.

accumulation in the spleen and liver yet rapid excretion from the bloodstream and tumors (Fig. 4A), whereas ^{177}Lu-FAP6-IP-DOTA readily cleared from healthy organs despite its protracted retention in blood and tumors (Fig. 4B). The data thus confirm that insertion of an iodophenyl albumin binder facilitates FAP6 circulation in the bloodstream, thereby avoiding premature capture by excretory organs, enabling increased FAP6 uptake by the CAFs and, ultimately, saturation of the tumor. Dosimetry estimates (Supplemental Fig. 10), ^{177}Lu-FAP6-IP-DOTA SPECT/CT scans, and ^{111}In-FAP6-IP-DOTA biodistribution studies were also performed (Supplemental Fig. 11; Supplemental Table 1).
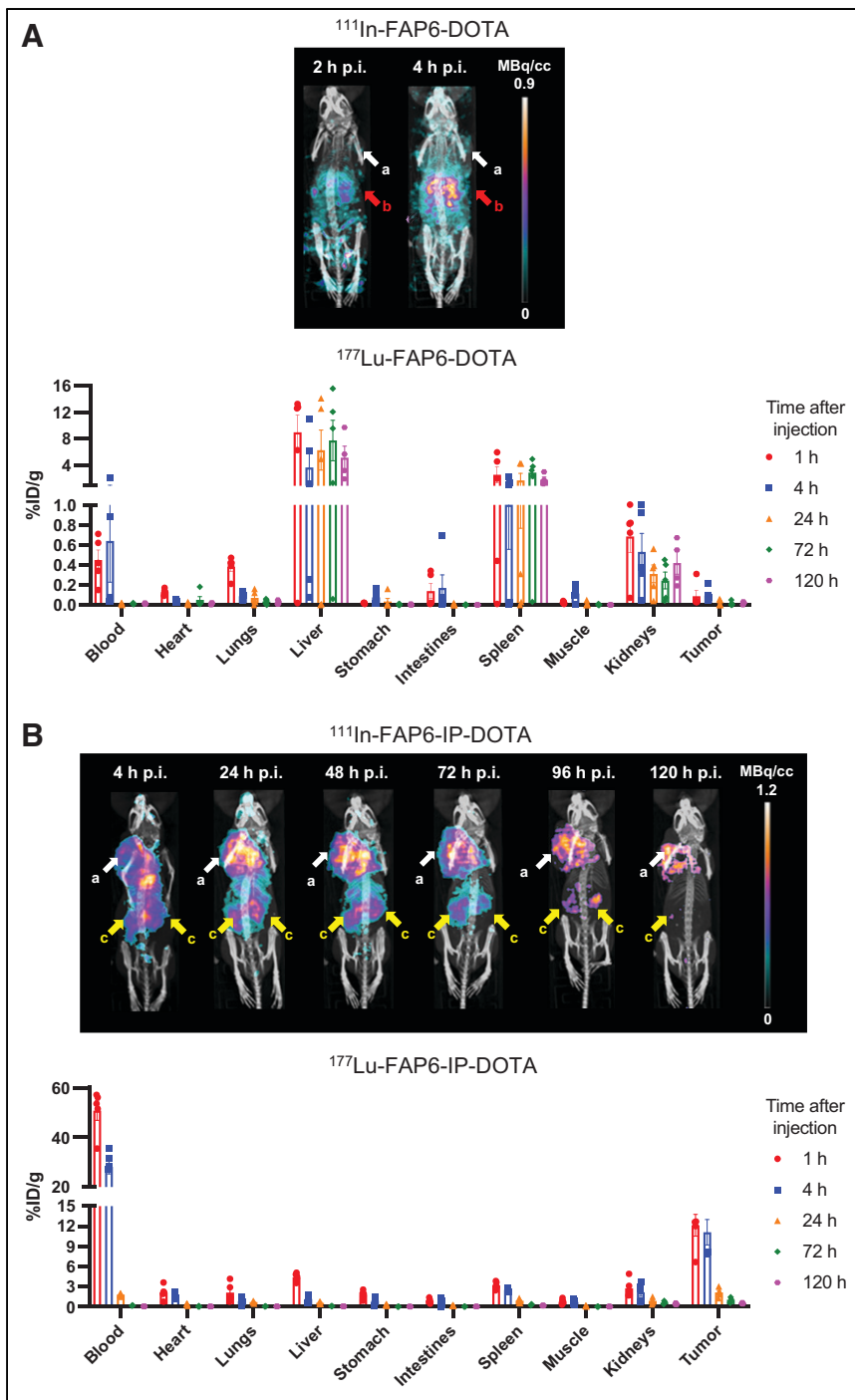
Effect of Albumin Binder on Radiotherapeutic Potencies of FAP6 RLTs

Encouraged by the improved tumor accumulation conferred by insertion of an albumin binder, we next compared the radiotherapeutic potencies of the 2 FAP-targeted RLTs. Moreover, to expand the diversity of tumor types in which the FAP-targeted RLTs would be compared, we used a human cancer xenograft model (KB cells) reported to respond to radiotherapy (7) and in which the only cells overexpressing FAP were again CAFs (13,14). Mice bearing tumors generated from FAP-negative KB cells were injected intravenously with a single dose of vehicle alone or with ^{177}Lu-FAP6-DOTA or ^{177}Lu-FAP6-IP-DOTA on day 0. Tumor sizes and body weights were then measured every other day for 10 wk.

Consistent with the above SPECT/CT and biodistribution results, ^{177}Lu-FAP6-DOTA provided no therapeutic benefit, suppressing tumor growth by only 3% and conferring no prolongation of overall survival (Fig. 5A). In contrast, ^{177}Lu-FAP6-IP-DOTA radiotherapy suppressed tumor growth by about 36% and improved overall survival by an average of about 3 wk (Fig. 5B, P = not statistically significant). Although mice treated with ^{177}Lu-FAP6-IP-DOTA experienced minor weight loss immediately after injection, the same mice quickly recovered and displayed no persisting toxicities, as also is consistent with the clearance of ^{177}Lu-FAP6-IP-DOTA from healthy tissues.

transient retention was also observed in the kidneys, the absence of significant accumulation in the liver suggested that FAP6-IP-DOTA might constitute an RLT worthy of further scrutiny.

To confirm these results, we next quantitated the biodistributions of each FAP6 conjugate in separate cohorts of 4T1 tumor–bearing mice over time. ^{177}Lu-FAP6-DOTA demonstrated prolonged

Evaluation of ^{177}Lu-FAP6-IP-DOTA Treatment in Multiple Tumor Types

Satisfied that ^{177}Lu-FAP6-IP-DOTA constituted the better FAP-targeted RLT, we next investigated whether ^{177}Lu-FAP6-IP-DOTA might effectively treat a diversity of solid tumors, as frequently envisioned by others (3,18). Mice bearing HT29, U87MG, or 4T1

FIGURE 4. SPECT/CT and biodistribution analyses of FAP6-DOTA (A) vs. FAP6-IP-DOTA (B) in 4T1 tumors. %ID = percentage injected dose; a = tumors; b = liver; c = kidneys; p.i. = after injection.
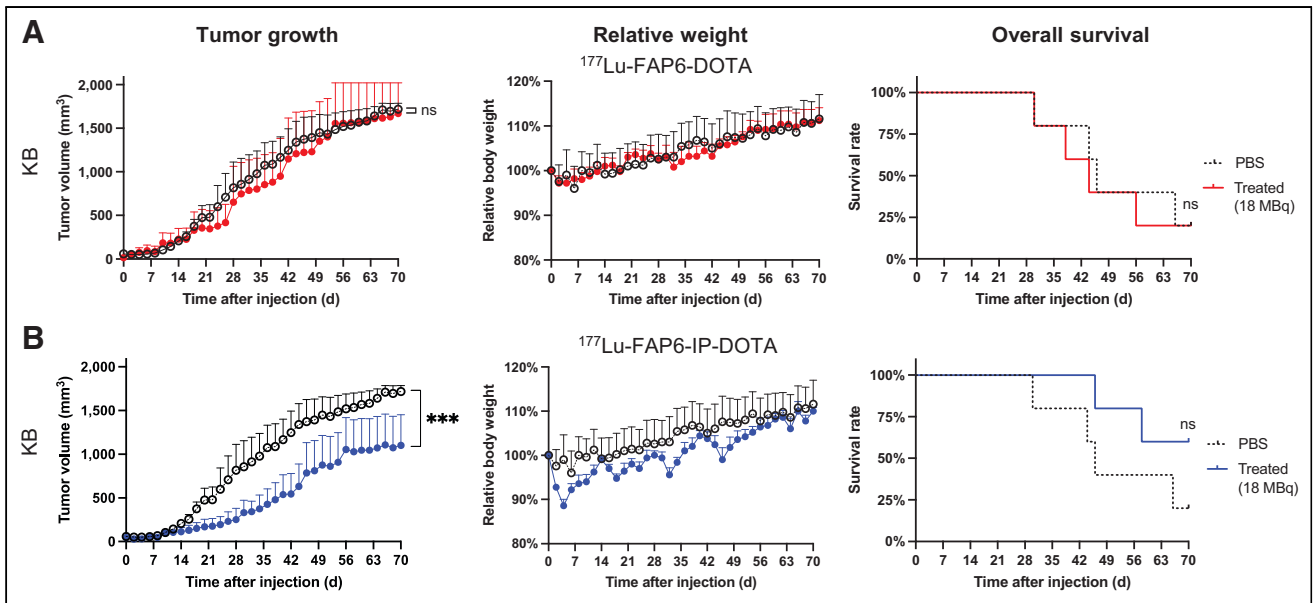
cohorts of 5 mice per group were injected with 18 MBq of ^{177}Lu-FAP6-IP-DOTA and monitored. Growth of U87MG tumors was reduced by about 41% (Fig. 6B), but 4T1 tumors again continued to grow unabated (Supplemental Fig. 12B). Finally, 4T1 tumors treated with 55 MBq of ^{177}Lu-FAP6-IP-DOTA responded with an approximately 43% decrease in growth (Fig. 6C). Overall survival was significantly prolonged by at least 12 d at the respective doses without inducing persistent weight loss.

To further explore the potential toxicity of a single dose of ^{177}Lu-FAP6-IP-DOTA, tissues from mice treated with 18 or 55 MBq were prepared for histologic examination. No diagnostic lesions or other significant morphologic differences between treated and control mice were identified (Supplemental Table 2). Hepatic extramedullary hematopoiesis and increases in circulating neutrophils were observed in several of the mice treated with 18 MBq, but this finding is expected in mice regardless of the treatment received (26). Surprisingly, mice treated with 55 MBq showed fewer histopathologic changes in the heart and liver than did untreated controls. Although mild lesions were observed in several kidneys, the lesions were deemed nonspecific (representative photomicrographs of tissue sections after both doses are shown in Supplemental Fig. 13). One lesion observed in the myocardium of a mouse 21 d after treatment with a 55-MBq dose revealed mineralization and epicarditis. Although this inflammation may be drug-related, carditis can be simply spontaneous (27). The minimal radioactivity in the heart and the mouse's healthy weight gain both raise a question regarding any causal relationship between the treatment and the lesion. Taken together, these data demonstrate that the radiation doses used here were able to suppress tumor growth without causing acute tissue changes.

DISCUSSION

Most preclinical studies of FAP-targeted imaging and therapeutic agents to date have used murine tumor models in which the cancer cells themselves directly express FAP (19,20,28–34). As shown in Figure 2, FAP is either absent or weakly expressed on malignant cells from breast, lung, colorectal, and ovarian human cancer patients. Although tumor models derived from cancer cells that were transduced to overexpress FAP can be useful for proof-of-concept studies, their high FAP expression may also obscure a need to modify the molecular design of an RLT to increase tumor accumulation in humans, such as by the addition of an albumin

tumors were injected intravenously with a single dose of either vehicle alone or vehicle with ^{177}Lu-FAP6-IP-DOTA on day 0, after which tumor sizes and body weights were measured every other day. Growth of HT29 tumors was suppressed by about 58% by 9 MBq of ^{177}Lu-FAP6-IP-DOTA (Fig. 6A), but surprisingly, this dose did not affect U87MG or 4T1 tumors (Supplemental Figs. 12A and 12B). To determine whether U87MG or 4T1 tumors might respond to a higher dose of ^{177}Lu-FAP6-IP-DOTA, additional

FIGURE 5. Treatment of KB tumors with ^{177}Lu-FAP6-DOTA (A) or ^{177}Lu-FAP6-IP-DOTA (B) ($n = 5$/group). PBS = phosphate-buffered saline.
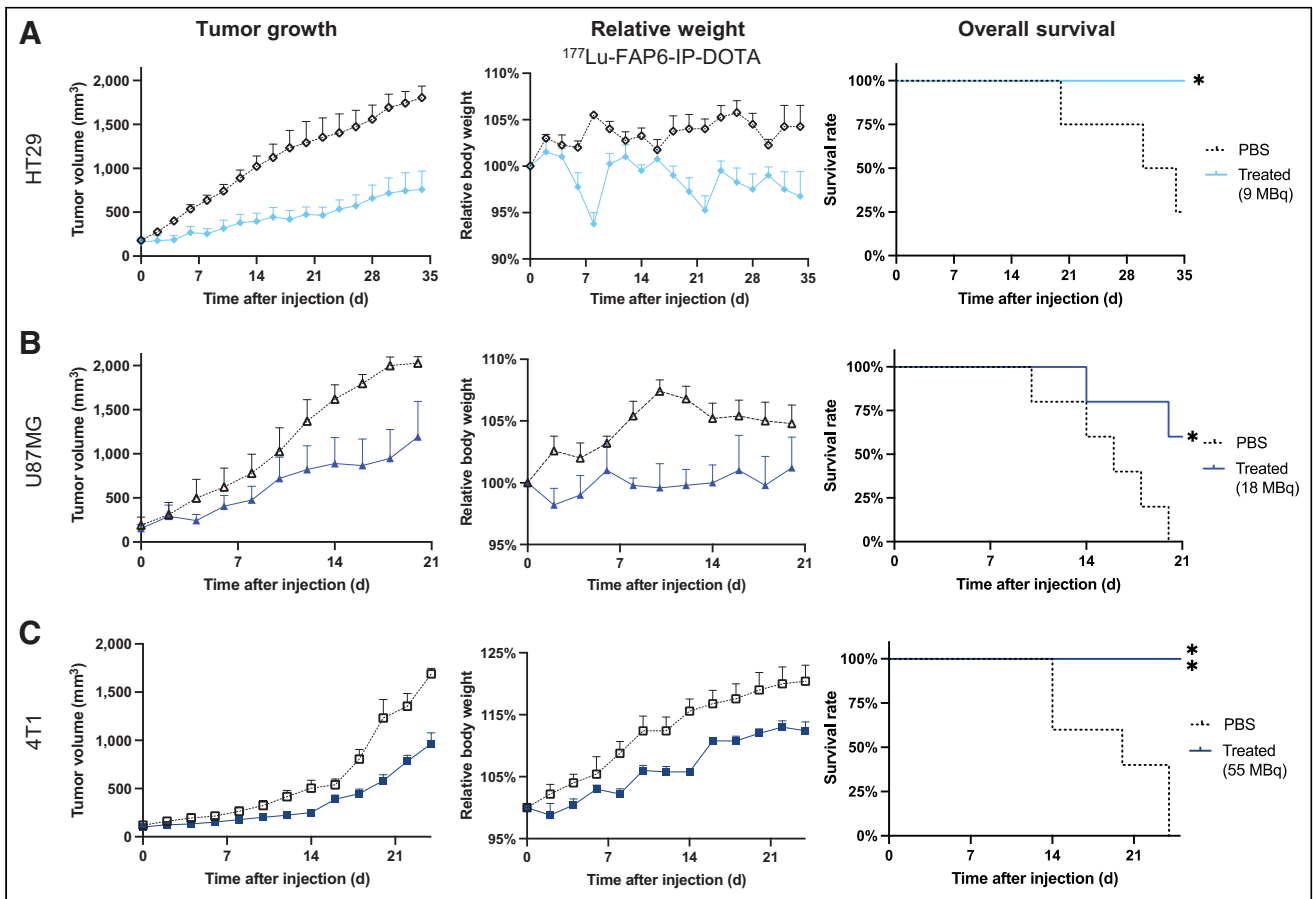
FIGURE 6. Treatment of HT29 ($n = 4$/group) (A), U87MG ($n = 5$/group) (B), or 4T1 ($n = 5$/group) (C) tumors with ^{177}Lu-FAP6-IP-DOTA. PBS = phosphate-buffered saline.

binder. Tumor models with physiologically relevant levels of FAP expression should therefore be encouraged in RLT studies intended for clinical development.

It was noteworthy that our 4 tumor models displayed different sensitivities to ^{177}Lu-FAP6-IP-DOTA, according to the ranking HT29 > U87MG ≈ KB > 4T1 tumors. Although variations in FAP expression will directly influence initial uptake of our RLT and may account for some of these different radiotherapy responses, no clear correlation was observed with in vivo FAP staining intensity (Supplemental Fig. 2). Discrepancies in intrinsic resistance mechanisms such as DNA damage repair pathways may help clarify the observed radiosensitivities in vivo, but analysis of the growth of the 4 cancer cell lines in vitro after radiation exposure also did not reveal a direct correlation (Supplemental Fig. 14). Considering that additional characteristics such as growth rates, vascularization, extracellular matrix densities, drug efflux pumps, and CAF distributions can all influence radiobiology (35), we suspect that no single variable will account for the disparities observed in these 4 tumor models. One limitation of this work is that preclinical radiotherapy studies typically translate poorly into humans because of alterations of such characteristics in murine tumor models (36). For future RLT studies on mice to predict response rates more reliably in humans, it will be important to identify tumor models that more accurately mimic the radiation resistance mechanisms and general biology of human cancers.

Motivated by previous successes in using a FAP6 near-infrared dye conjugate to image 7 different murine tumor models (13), we attempted to adapt the same FAP6 ligand as a radiopharmaceutical. Although the inability of FAP6-DOTA to concentrate in tumors generated by FAP-negative 4T1 cells may seem initially surprising, it should be noted that Watabe (18) and Slania (25) also observed minimal uptake with FAPI conjugates when imaging pancreatic and prostate tumor models, respectively, in which the cancer cells did not directly express FAP. Because FAP6 exhibits higher affinity for FAP than FAPI (19,20,32), is readily internalized by an endocytic mechanism (32), and did not show tumor accumulation even when high mass doses of compound were administered (Supplemental Fig. 6), we hypothesized that the lack of tumor uptake of FAP6-DOTA was due to its rapid excretion before sufficient perfusion into the tumors. Therefore, to prolong the circulation, we inserted the iodophenyl butyryl moiety to generate FAP6-IP-DOTA, which accumulated prominently in 4T1 tumors. The net effect was an approximately 88-times increase in tumor dose, more than a 1,500-times improvement in tumor–to–total-body dosimetry ratio (Supplemental Fig. 10), and effective radiotherapy of 4 tumor models.

Whether greater improvements can still be achieved with better FAP ligands (14,37), albumin binders (34,38), or linker modifications (20,23,32) is a question worthy of further scrutiny. The dosimetry estimates of FAP6-IP-DOTA revealed most tumor–to–healthy-organ ratios to be favorable (Supplemental Fig. 10), but the 2:1 tumor-to-kidney ratio may require additional improvement (39). This can be achieved by altering the albumin binder as described by others (38,40), but one limitation of drug development is that translating optimal pharmacokinetics in mice to humans is complicated by differences in metabolism and excretion (10). Another aspect of drug development is evaluating the performance of the FAP6-IP-DOTA candidate with respect to other FAP-targeted RLTs. FAP6-IP-DOTA demonstrates tumor retention seemingly superior to that of FAPI-46, as well as clearance from healthy organs faster than that of other FAP-targeted albumin-binding radioligands (19,20,30,32). However, direct comparisons should be limited because most other studies used different tumor models in which the cancer cells directly overexpressed FAP and necessitated immunocompromised mouse strains. What structural elements result in optimal properties for FAP-targeted RLT in humans remains an important question for research.

Finally, it should be noted that tumors characterized by lower numbers of FAP-positive cells may still be less responsive to an optimized FAP-targeted RLT. Thus, successful treatment of some solid tumors may require combination with conventional therapies, combination with an orthogonal RLT targeted to other cells in the same tumor, or use of a FAP-targeted radioimaging companion diagnostic to select only patients with high FAP expression for radiotherapy (5,41). With these improvements, it remains conceivable that a FAP-targeted RLT may prove useful for treatment of many solid tumors.

CONCLUSION

To design a more clinically relevant study, 4 different tumor models with ostensibly physiologic (i.e., lower) levels of FAP expression were selected after analysis of scRNA-seq data from human cancers. The FAP6-IP-DOTA molecule demonstrated high affinity for FAP and prolonged circulation, resulting in strong accumulation in all 4 tumors and significant suppression of tumor growth when radiolabeled with [177]Lu. The data suggest that ^{177}Lu-FAP6-IP-DOTA may potentially be optimized for human use.

DISCLOSURE

ACKNOWLEDGMENTS

KEY POINTS

QUESTION: Can a FAP-targeted radioligand therapy demonstrate sufficient safety and efficacy for preclinical development in murine tumor models in which FAP expression is limited to CAFs?

PERTINENT FINDINGS: scRNA-seq data on 34 human breast, lung, ovarian, and colon cancers demonstrated that about 5% of all cells in human tumors overexpress FAP. ^{177}Lu-FAP6-IP-DOTA successfully treated multiple murine tumor models generated from FAP-negative cancer cells.

IMPLICATIONS FOR PATIENT CARE: These data suggest that ^{177}Lu-FAP6-IP-DOTA constitutes a promising candidate for development of FAP-targeted radiotherapy for solid tumors.

REFERENCES

1. Liu R, Li H, Liu L, et al. Fibroblast activation protein: a potential therapeutic target in cancer. *Cancer Biol Ther.* 2012;13:123–129.

2. Garin-Chesa P, Old LJ, Rettig WJ. Cell surface glycoprotein of reactive stromal fibroblasts as a potential antibody target in human epithelial cancers. *Proc Natl Acad Sci USA.* 1990;87:7235–7239.

3. Kratochwil C, Flechsig P, Lindner T, et al. ^{68}Ga-FAPI PET/CT: tracer uptake in 28 different kinds of cancer. *J Nucl Med.* 2019;60:801–805.

4. Ferdinandus J, Costa PF, Kessler L, et al. Initial clinical experience with ^{90}Y-FAPI-46 radioligand therapy for advanced-stage solid tumors: a case series of 9 patients. *J Nucl Med.* 2022;63:727–734.

5. Baum RP, Schuchardt C, Singh A, et al. Feasibility, biodistribution, and preliminary dosimetry in peptide-targeted radionuclide therapy of diverse adenocarcinomas using ^{177}Lu-FAP-2286: first-in-humans results. *J Nucl Med.* 2022;63:415–423.

6. Dumelin CE, Trüssel S, Buller F, et al. A portable albumin binder from a DNA-encoded chemical library. *Angew Chem Int Ed Engl.* 2008;47:3196–3201.

7. Müller C, Struthers H, Winiger C, et al. DOTA conjugate with an albumin-binding entity enables the first folic acid–targeted ^{177}Lu-radionuclide tumor therapy in mice. *J Nucl Med.* 2013;54:124–131.

8. Kuo H-T, Merkens H, Zhang Z, et al. Enhancing treatment efficacy of ^{177}Lu-PSMA-617 with the conjugation of an albumin-binding motif: preclinical dosimetry and endoradiotherapy studies. *Mol Pharm.* 2018;15:5183–5191.

9. Tian R, Jacobson O, Niu G, et al. Evans blue attachment enhances somatostatin receptor subtype-2 imaging and radiotherapy. *Theranostics.* 2018;8:735–745.

10. Kramer V, Fernández R, Lehnert W, et al. Biodistribution and dosimetry of a single dose of albumin-binding ligand [^{177}Lu]Lu-PSMA-ALB-56 in patients with mCRPC. *Eur J Nucl Med Mol Imaging.* 2021;48:893–903.

11. Qian J, Olbrecht S, Boeckx B, et al. A pan-cancer blueprint of the heterogeneous tumor microenvironment revealed by single-cell profiling. *Cell Res.* 2020;30:745–762.

12. SCope tutorial. Pan-Cancer TME Blueprint Website. http://scope.lambrechtslab.org/#/a0f9b96f-e2d9-4156-9899-993e37a62c03/Breast.loom/tutorial. Accessed January 4, 2023.

13. Mukkamala R, Lindeman SD, Kragness KA, et al. Design and characterization of fibroblast activation protein targeted pan-cancer imaging agent for fluorescence-guided surgery of solid tumors. *J Mater Chem B.* 2022;10:2038–2046.

14. Roy J, Hettiarachchi SU, Kaake M, et al. Design and validation of fibroblast activation protein alpha targeted imaging and therapeutic agents. *Theranostics.* 2020;10:5778–5789.

15. Cheng JD, Dunbrack RL Jr, Valianou M, et al. Promotion of tumor growth by murine fibroblast activation protein, a serine protease, in an animal model. *Cancer Res.* 2002;62:4767–4772.

16. Venning FA, Zornhagen KW, Wullkopf L, et al. Deciphering the temporal heterogeneity of cancer-associated fibroblast subpopulations in breast cancer. *J Exp Clin Cancer Res.* 2021;40:175.

17. Moon ES, Elvas F, Vliegen G, et al. Targeting fibroblast activation protein (FAP): next generation PET radiotracers using squaramide coupled bifunctional DOTA and DATA[5m] chelators. *EJNMMI Radiopharm Chem.* 2020;5:19.

18. Watabe T, Liu Y, Kaneda-Nakashima K, et al. Theranostics targeting fibroblast activation protein in the tumor stroma: [64]Cu- and [225]Ac-labeled FAPI-04 in pancreatic cancer xenograft mouse models. *J Nucl Med.* 2020;61:563–569.

19. Xu M, Zhang P, Ding J, et al. Albumin binder–conjugated fibroblast activation protein inhibitor radiopharmaceuticals for cancer therapy. *J Nucl Med.* 2022;63:952–958.

20. Wen X, Xu P, Shi M, et al. Evans blue-modified radiolabeled fibroblast activation protein inhibitor as long-acting cancer therapeutics. *Theranostics.* 2022;12:422–433.

21. Liu Y, Watabe T, Kaneda-Nakashima K, et al. Fibroblast activation protein targeted therapy using [^{177}Lu]FAPI-46 compared with [225]Ac]FAPI-46 in a pancreatic cancer model. *Eur J Nucl Med Mol Imaging.* 2022;49:871–880.

22. Kelly JM, Jeitner TM, Ponnala S, et al. A trifunctional theranostic ligand targeting fibroblast activation protein-α (FAPα). *Mol Imaging Biol.* 2021;23:686–696.

23. Meng L, Fang J, Zhao L, et al. Rational design and pharmacomodulation of protein-binding theranostic radioligands for targeting the fibroblast activation protein. *J Med Chem.* 2022;65:8245–8257.

24. Tsai T-Y, Yeh T-K, Chen X, et al. Substituted 4-carboxymethylpyroglutamic acid diamides as potent and selective inhibitors of fibroblast activation protein. *J Med Chem.* 2010;53:6572–6583.

25. Slania SL, Das D, Lisok A, et al. Imaging of fibroblast activation protein in cancer xenografts using novel (4-quinolinoyl)-glycyl-2-cyanopyrrolidine-based small molecules. *J Med Chem.* 2021;64:4059–4070.

26. Mende N, Laurenti E. Hematopoietic stem and progenitor cells outside the bone marrow: where, when, and why. *Exp Hematol.* 2021;104:9–16.

27. Glass AM, Coombs W, Taffet SM. Spontaneous cardiac calcinosis in BALB/cByJ mice. *Comp Med.* 2013;63:29–37.

28. Fischer E, Chaitanya K, Wüest T, et al. Radioimmunotherapy of fibroblast activation protein positive tumors by rapidly internalizing antibodies. *Clin Cancer Res.* 2012;18:6208–6218.

29. Zboralski D, Osterkamp F, Simmons A, et al. Preclinical evaluation of FAP-2286, a peptide-targeted radionuclide therapy (PTRT) to fibroblast activation protein alpha (FAP) [abstract]. *Ann Oncol.* 2020;31(suppl 4):S488.

30. Zhang P, Xu M, Ding J, et al. Fatty acid-conjugated radiopharmaceuticals for fibroblast activation protein-targeted radiotherapy. *Eur J Nucl Med Mol Imaging.* 2022;49:1985–1996.

31. Lindner T, Loktev A, Altmann A, et al. Development of quinoline-based theranostic ligands for the targeting of fibroblast activation protein. *J Nucl Med.* 2018;59:1415–1422.

32. Loktev A, Lindner T, Burger E-M, et al. Development of fibroblast activation protein–targeted radiotracers with improved tumor retention. *J Nucl Med.* 2019;60:1421–1429.

33. Galbiati A, Zana A, Bocci M, et al. A dimeric FAP-targeting small-molecule radioconjugate with high and prolonged tumor uptake. *J Nucl Med.* 2022;63:1852–1858.

34. Lin J-J, Chuang C-P, Lin J-Y, et al. Rational design, pharmacomodulation, and synthesis of [^{68}Ga]Ga-Alb-FAPtp-01, a selective tumor-associated fibroblast activation protein tracer for PET imaging of glioma. *ACS Sens.* 2021;6:3424–3435.

35. Henke E, Nandigama R, Ergün S. Extracellular matrix in the tumor microenvironment and its impact on cancer therapy. *Front Mol Biosci.* 2020;6:160.

36. Koontz BF, Verhaegen F, De Ruysscher D. Tumour and normal tissue radiobiology in mouse models: how close are mice to mini-humans? *Br J Radiol.* 2017;90:20160441.

37. Hettiarachchi SU, Li Y-H, Roy J, et al. Targeted inhibition of PI3 kinase/mTOR specifically in fibrotic lung fibroblasts suppresses pulmonary fibrosis in experimental models. *Sci Transl Med.* 2020;12:eaay3724.

38. Kuo HT, Lin KS, Zhang Z, et al. ^{177}Lu-labeled albumin-binder-conjugated PSMA-targeting agents with extremely high tumor uptake and enhanced tumor-to-kidney absorbed dose ratio. *J Nucl Med.* 2021;62:521–527.

39. Emami B, Lyman J, Brown A, et al. Tolerance of normal tissue to therapeutic irradiation. *Int J Radiat Oncol Biol Phys.* 1991;21:109–122.

40. Umbricht CA, Benešová M, Schibli R, et al. Preclinical development of novel PSMA-targeting radioligands: modulation of albumin-binding properties to improve prostate cancer therapy. *Mol Pharm.* 2018;15:2297–2306.

41. Fendler WP, Pabst KM, Kessler L, et al. Safety and efficacy of ^{90}Y-FAPI-46 radioligand therapy in patients with advanced sarcoma and other cancer entities. *Clin Cancer Res.* 2022;28:4346–4353.